Biomedical Microdevices 5:2, 101–108, 2003

Hybrid Bio/Artificial Microdevices:

Section Editors Dr Sangeeta Bhatia and Dr Christopher Chen

Micro/nanomachining of Polymer Surface for Promoting Osteoblast Cell Adhesion

Wei He,[2] Kenneth E. Gonsalves,[1] Nikola Batina,[3] Dave B. Poker,[4] Emily Alexander,[5] and Michael Hudson[5]*

E-mail: kegonsalves@email.uncc.edu
[1]Department of Chemistry and Cameron Applied Research Center, University of North Carolina, Charlotte, NC
[2]Department of Chemistry, University of Connecticut, Storrs, CT
[3]Departmento de Quimica, Universidad Autonoma Metropolitana-Iztapalapa, Mexico D.F., Mexico
[4]Oak Ridge National Laboratory, Oak Ridge, TN
[5]Department of Biology, University of North Carolina, Charlotte, NC

Abstract. **Interactions between cells and biomaterials are affected by surface properties. Therefore, various approaches have been introduced for surface modifications. Here a technique based on ion beam lithography to improve osteoblast cell adhesion on polymeric materials is reported. We have demonstrated that exposing the polymer to P^+ or Ar^+ ions through masks can generate micro/nano-scale patterns. Our results illustrate that after exposure to an ion beam, the amount of osteoblast cells attached to the polymer was enhanced as a consequence of the roughened surface as well as due to the implanted ions. This indicates that masked ion beam lithography (MIBL) can not only generate nanostructures on the surface of a biocompatible polymer, but can also selectively modify the surface chemistry by implanting with specific ions. These factors can contribute to an osteogenic environment.**

Key Words. **bone tissue engineering, ion implantation, polymers, osteoblast cells, micromachining**

1. Introduction

Bone is one of the intensively investigated areas for tissue engineering replacement alternatives (Laurencin et al., 1999). According to the National Center of Health Statistics, greater than two billion dollars are spent annually in the United States alone on bone related implants including hip replacements, knee replacements, dental implants, and pins to stabilize or repair fractures (http://www.cdc.gov/nchs). Bone is a highly vascular, mineralized connective tissue consisting of cells embedded in a matrix composed of organic material and inorganic salts rich in calcium and phosphate. It is an extremely complex tissue that provides many vital functions in the body (Sikavitsas et al., 2001). Thus, bone tissue engineering holds great potential in providing strategies that will result in complete regeneration of bone and restoration of its function. As a class of biomaterials, metals are perhaps the most widely used for implants. For instance, some of the most common orthopedic surgeries involve the implantation of metallic implants. These range from simple wires and screws to fracture-fixation plates and total joint prostheses (artificial joints) for hips, knees, shoulders, elbows, etc. (Agrawal, 1998). In the field of orthopedics, metals are popular primarily because of their ability to bear significant loads, withstand fatigue loading, and undergo plastic deformation prior to failure. Currently, the most commonly used metals for orthopaedic implants include stainless steels, cobalt-chromium-molybdenum alloys, commercially pure titanium, and titanium alloys (Agrawal, 1998). A rapidly established, strong and long lasting connection between an implant and bone is essential for the clinical success of orthopeadic and dental implants. The morphology of an implant surface, including microtopography and roughness, has been shown to be an important factor in establishing such a reliable connection (Rich and Harris, 1981; Thomas and Cook, 1985; Buser et al., 1991; Wennerberg et al., 1996; Han et al., 1998). It appears that a frequent tissue response to smooth implant surfaces is the formation of a fibrous encapsulation (Thomas and Cook, 1985; Maniatopoulos et al., 1986; Chehroudi et al., 1989). It has been suggested that initial stability is more likely to

*Corresponding author.

be achieved with implants with rough surfaces and furthermore that bone-to-implant interfacial shear strength correlates positively with the degree of surface roughness (Webster et al., 2001; Lee et al., 1998). Therefore, rougher implant surface is preferred, and it can usually be prepared by methods such as coarse grit blasting, acid etching, wet sanding, plasma spraying, etc. (Lemons, 1998)

However, despite the generally successful application of metallic implants, problems do occur occasionally. One of the primary concern of these metallic implants is their tendency to release metallic ions, which would act as potential allergy or toxicity sources due to their known toxic effects on human cells (Bosetti et al., 2001; Bianchi et al., 1980; Heath et al., 1967; Hanawa et al., 1999). The other problem with metallic implants is that the interaction between bone and the implant does not involve a chemical bond. The lack of ability to bond chemically may lead to slow fixation of the implants and to their gradual loosening over a long period. Mechanical loosening of implants from the bone can result in excessive joint displacement and generally mandates the need for revision surgery which is more difficult, less successful, causes additional damage to surrounding tissues and is economically frustrating (Dwayne and McCain, 2000). Obviously, it would be more desirable to eliminate the second surgical procedure to minimize patient pain, chance of infection, and subsequent trauma to the newly healed site. More recently, new treatment methods and improved materials, including non-metallic implants, have been used to treat bone defects (Trieu et al., 2000). The non-metallic implants can be made of materials that biodegrade over a time period ranging from a few days to several months. Although the progress is promising, further development is necessary to improve bone adherence and mediate proper interface formation by bone ingrowth while maintaining enough mechanical properties.

In this study, a novel approach, namely masked ion beam lithography (MIBL), was explored for surface modification of non-metallic materials for bone related applications. Ion implantation is mainly used in the semiconductor manufacturing process. It has played a steadily increasing role in production processes for leading-edge integrated circuit fabrication, due to its flexibility in the selection of dopant species, their spatial location within the device, and in subtle control of the concentration profile (Nishi and Doering, 2000). It also has been used to improve surface properties of metals, such as wear and corrosion resistance (Bosetti et al., 2001; Hanawa et al., 1997). In recent years it has been reported that ion beam irradiation of polymers can improve cell adhesion (Suzuki et al., 1992; Bacakova et al., 1996; Pignataro et al., 1997; Lhoest et al., 1995) and blood compatibility (Li et al., 1999). The potential advantages of using ion implantation as a microfabrication technique are: (a) since it is a one-step process, the patterns can be ''micromachined'' into the material in a controled manner through masks; (b) by selecting the right ions to implant, such as Ca or P, the surface chemistry of the biocompatible material can be tailored, which may influence certain biological processes (Boyan et al., 1996). This paper reports on micro/nano machining of poly(methyl methacrylate) (PMMA) surfaces by masked ion lithography, specifically, by P^+ ions and Ar^+ ions, leading to well-defined microwells and improved osteoblast cell adhesion.

2. Material and Methods

2.1. Ion implantations

The PMMA film was prepared as described previously (He et al., 2002). A fine nickel mesh obtained from Buckbee-Mears, St. Paul, MN served as a mask. The mask had a maximum transmittance of 36% and the space between the wires was 7.62 μm. A piece of $0.7'' \times 0.7''$ mesh was placed on the PMMA film using copper tape.

Implantations were applied to the samples on an Extrion implant accelerator, a general purpose Cockcroft-Walton-type ion implanter with a modified Freeman source, at the Surface Modification and Characterization Research Center at Oak Ridge National Laboratory, TN. The implants were performed by raster scanning the ion beam over a circular implant area of about $4\,cm^2$ area. This assures a uniform implanted dose over the entire implant area. Samples were clamped to a sample holder that was maintained near room temperature. The sample holder was biased to + 67 volts to suppress secondary electron emission, and was surrounded by a Faraday cage at − 300 volts for both secondary electron suppression and secondary ion collection. The absolute accuracy with suppression is generally better than 10%. However, the linearity is much better, usually better than 1%. The sample current was measured as the sum of the current on the sample holder and the suppressor. P^+ ion implantation was carried out at an energy of 85 keV with ion fluences of 1×10^{15} ions/cm^2. Also Ar^+ ion implantation was done at an energy of 115 keV with ion dosage of 1×10^{15} ions/cm^2.

2.2. Surface characterization

After the implantations, the meshes were removed and the PMMA films were characterized using the following methods:

- Atomic force microscopy (AFM): Surface morphology examinations were conducted by AFM. Imaging was performed at room temperature using a commercial optical lever microscope (Nanoscope III, Digital Instruments). Standard-geometry silicon nitride probes (TESP) tips 125 μm in length and with a typical frequency between 294 and 375 kHz were used (Digital Instruments). Tapping mode topographic images were taken in air in the constant deflection mode, with a very slow scan rate of 1 Hz which provided less contact between the AFM tip and the imaged sample, leaving the sample surface in its intact mode.
- X-ray photoelectron spectroscopy (XPS) investigation was performed with a Riber LAS-3000 system. Electron ejection from the samples was induced by $12\,\text{kV} \times 15\,\text{mA}$ Mg K_α X-ray radiation at a pass energy of 20 eV and a step size of 0.1 eV. The pressure in the sample chamber was kept below 1×10^{-9} Torr. Charging of the samples, due to photoemission, was corrected by setting the energy of the main hydrocarbon component of C_{1s} spectra at 285.0 eV.
- Dynamic secondary ion mass spectroscopy (SIMS) measurement was carried out using a PHI Quadrupole SIMS instrument (Physical Electronics, Inc.) with a cesium primary beam at an impact energy of 3 keV. The primary ion angle of incidence was 60°. Charge neutralization was applied.

2.3. Cell culture and cell attachment assay

Normal osteoblast cell cultures were prepared from mouse neonates according to a method previously described for chick embryos (Ramp et al., 1994). Bone-forming cells were isolated from mouse neonate calvariae by sequential collagenase-protease digestion. The isolated cells were pooled in mouse osteoblast growth medium (OBGM) consisting of Dulbecco's modified Eagle's medium with 25 mM HEPES, 10% fetal bovine serum, 2 g/L sodium bicarbonate, 75 μg/ml glycine, 100 μg/ml ascorbic acid, 40 ng/ml vitamin B_{12}, 2 μg/ml *p*-aminobenzoic acid, 200 ng/ml biotin, and 100 U/ml-100 μg/ml-0.25 μg/ml penicillin-streptomycin-fungizone (pH 7.4) (Ramp et al., 1991). Cells were then seeded into 25 cm^2 flask at a density of 10^6 osteoblasts/flask and incubated at 37 °C in a 5% CO_2 atmosphere until they reached approximately 80% confluency. Ostocalcin, type I collagen, and alkaline phosphatase were selected to characterize isolated mouse osteoblasts. Measurement of osteoblast attachment to the various surfaces was performed essentially as previously described (Dalton et al., 1996). Media was removed from flasks containing osteoblasts, and the osteoblasts were rinsed with Hank's balanced salt solution (HBSS). Osteoblasts were then metabolically-labeled by culturing for 18 hours in OBGM labeling medium containing methionine-free Dulbecco's modified Eagle's medium supplemented with [^{35}S] methionine (Translabel 51,006; ICN Biomedicals, Costa Mesa, CA, USA) at a concentration of 0.185 MBq/mL (5 μCi/ml). Following the 18 hours labeling period, media was removed from osteoblast cultures, and osteoblasts were rinsed with HBSS. Osteoblast cells were detached, resuspended, and seeded into 6-well cluster plate. PMMA samples irradiated to P^+ and Ar^+ ions were placed in the well. Pristine PMMA was used as control. The seeding density was 150,000 cells per well. After incubation at 37 °C in a 5% CO_2 atmosphere for 24 hours, the culture plate was rinsed three times with HBSS. The plate was then allowed to air dry. Samples were exposed to a Kodak storage phosphor screen (SO230; Molecular Dynamics, Sunnyvale, CA, USA) for 2 hours, and protected from light during that time. The screen was then scanned in a Typhoon 8600 Variable Mode PhosphorImager (Molecular Dynamics), which converts regions of higher energy in the screen to a digital image, in which pixel values are equivalent to energy levels. Using ImageQuant software (version 5.2) (Molecular Dynamics) a grid was created and superimposed over the area representative of each wafer as previously described (Dalton et al., 1996). An ImageQuant program was used to quantify the pixel values in each grid (as described in ImageQuant Users Guide). The results were the mean and standard deviation of pixel values.

3. Results

Poly (methyl methacrylate) (PMMA) has been used as a biomaterial (Lampin et al., 1997), for example, it is used extensively as bone cement which is primarily used to support the stems of total joint prostheses in the medullary cavity of bone (Agrawal, 1998). It was selected in our study as a model system because of its biocompatibility. A uniform PMMA film was formed by spin-casting PMMA solution on a silicon wafer. The film was 217 nm thick as measured by the Tencor Alphastep 200 surface profilometer.

The PMMA films were then subjected to MIBL. A schematic illustration of the process is given in Figure 1. The ions that were used in the MIBL process were phosphorous ions and argon ions, respectively. It has been shown previously that calcium phosphate forms spontaneously on the surface of titanium in the solution simulating physiological fluids (Sundgren et al., 1986; Hanawa and Ota, 1991). It is this layer that makes titanium biocompatible. Hanawa et al. (1993) and Hanawa and Ota (1992) have demonstrated that calcium

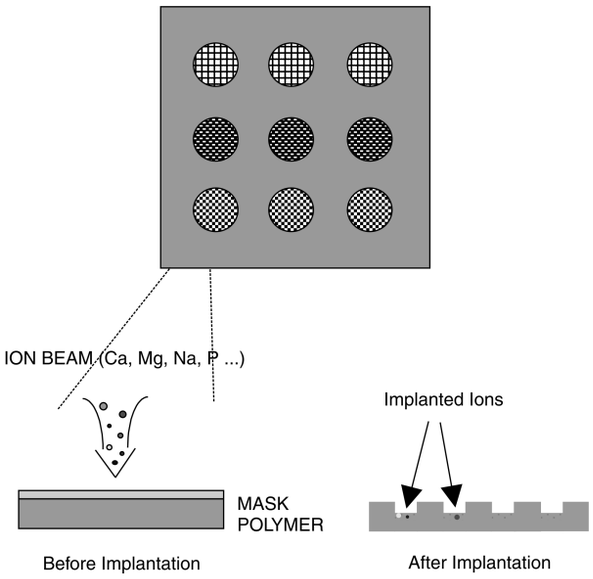

Fig. 1. Schematic illustration of the masked ion beam lithography (MIBL) process.

ion implantation of titanium can accelerate the formation of calcium phosphate on the titanium surface. Since phosphorous is a constituent of phosphates, it was selected as the ion species in our study (Krupa et al., 2002). In order to determine whether the implanted ion species have any effect on bone cell adhesion, inert argon ions were also chosen for comparison.

Irradiation with energetic ions leads to dramatic modification of polymer surfaces. The ions penetrate the surface and create significant changes by interacting with the polymer atoms via electronic (ionization) and nuclear (recoil) interactions (Chu et al., 2002). The thickness of the modified layer and the degree of structural changes depend on the ion mass and energy. The ion energies applied in P^+ ion implantation and Ar^+ ion implantation were chosen to ensure approximately the same projected range for both ion species in PMMA.

Following exposure to ion beams, simply removing the mask without any further treatment of the polymer revealed the patterns that were generated during the processes. Such unique feature provides a potential replacement of MIBL with conventional photolighography because most chemicals used in standard photolithography are toxic to cells and can denature biomolecules. There are some drawbacks for the application of photolithography to biopatterning.

It is known that changes in surface morphology can affect the interaction between cell and the material, such as cell adhesion and proliferation. The surface morphology of the PMMA film was studied using AFM after ion irradiation. Images presented in Figures 2 and 3 show 3-dimensional sample topography with patterns of very defined shape, which are distributed uniformly over the image area. In such topographic types of images, the upper part of the surface is presented by a lighter color. The observed patterns were characterized in detail by determination of the surface roughness, shape and distributions of surface profiles.

The AFM results of cross section analysis on the P^+ ions (85 keV, 1×10^{15} ions/cm^2) irradiated sample showed that the distance between the isolated islands is about 9.8 μm, and the height of each island is about 129 nm (Figure 2). It can be seen from the cross section analysis that the hole is of a conical shape. The width at the top of the hole is slightly larger than that of the bottom. It was also observed that the walls around the surface openings (holes) were not the same on all sides. It seems that along the shorter sides of the rectangular openings the walls are about 40% thicker than in the other directions. In order to verify such phenomena, images obtained by scanning the AFM tip in different directions were collected. It was concluded that the shape of the patterns and walls, in a qualitative and quantitative sense, do not depend on the scan direction during imaging.

The conditions used in Ar^+ ion implantations were chosen based on calculation from TRIM program (Ziegler et al., 1985), such that the resulted projection range would be similar to that achieved in P^+ ion implantations. The experimental results were in good agreement with the prediction. As shown in Figure 3, arrays of wells were observed uniformly distributed on the PMMA surface that has been exposed to 115 keV, 1×10^{15} ions/cm^2 Ar^+ ions. Similar to the patterns created with lower dose exposure of P^+ ions (Figure 2), the walls around the wells were not the same on all sides. Cross section analysis with AFM showed that the distance between the islands was 11.5 μm, and the depth 133 nm.

It has been observed that the effect of ion implantation on the material is confined to a very thin layer beneath the surface, usually less than a micrometer (Chu et al., 2002). Therefore, nano-size features can be achieved by properly selecting the energy of the ion beam. Besides surface profile, surface roughness of each sample was also determined in the AFM studies by measuring the root mean square roughness (R_{rms}). As shown in Table 1, R_{rms} of the PMMA surfaces after exposured to ion implantations was around 60 nm. As expected from the TRIM program, similar rough surfaces were achieved for both P and Ar ion implantations. The PMMA surface exposed to P^+ ions was a little bit rougher in contrast to the Ar^+ ions irradiation. This finding could be explained by a larger effect of the heavier Ar^+ on the PMMA chemical structure which in turn may lead to a decrease

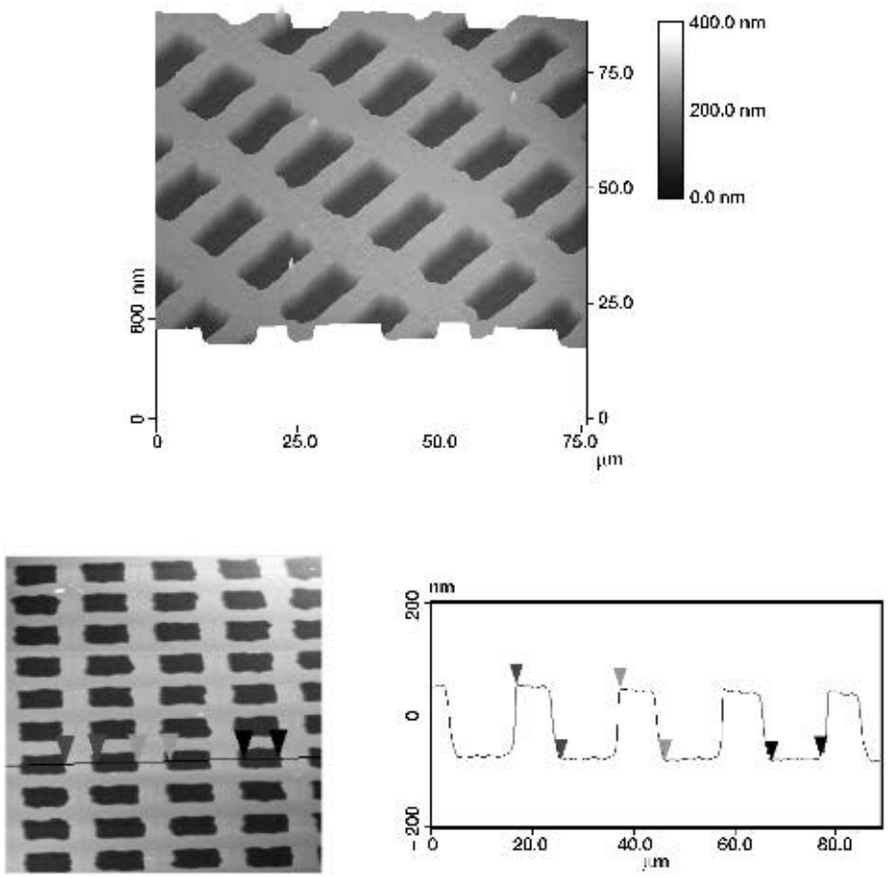

Fig. 2. *AFM images of the PMMA surfaces after exposure with 85 keV, 1×10^{15} ions/cm^2 P^+ ions, recorded in the tapping mode with typical surface features characterized by a cross section analysis.*

of free volume fraction in the PMMA surface layer and subsequent densification and compaction (Švorčík et al., 2000).

To study how ion implantation affects the chemical properties of the substrate, surface chemical state comparison using XPS was conducted to reveal the difference between the pristine and P^+ implanted PMMA samples with the fluence of 1×10^{15} ions/cm^2. Figure 4 represents characteristic C_{1s} (285 eV) and O_{1s} (535 eV) XPS signals. It can be seen in the XPS survey spectra obtained under low spectral resolution conditions that the O_{1s} peak relative intensity decreases in going from the pristine (spectrum a) to the P^+ ions implanted sample (spectrum b). The change in the relative amount of oxygen is caused by the loss of the O-containing pendant methylester groups. To further prove the cleavage of some pendant groups, C_{1s} signals were measured. As seen in Figure 5, the decrease of the 288.5 eV component of the C_{1s} peak, which is associated with carbons of the O—C═O groups, testifies to the destruction of the methylester groups from the polymer backbone.

In order to evaluate the influence of the ion beam treatments on cell adhesion, rat calvaria osteoblast cells were seeded on unirradiated and irradiated PMMA surfaces. These osteoblast cells were metabolically labeled with [^{35}S]-methionine. Following 24 hours incubation, the samples were rinsed in HBSS to remove non-adherent cells, dried, and phosphor-screen autoradiography was carried out. The images were developed and the pixel values were quantified, which were proportional to the amount of osteoblast cells attached (Dalton et al., 1996). For easy comparison, relative intensity was calculated referring to the pixel values determined on the pristine PMMA sample. As shown in Table 1, significant differences were observed in osteoblastic cells' responses to PMMA exposed to ion irradiation. Both P^+ ions implanted and Ar^+ ions implanted PMMA samples have more cells attached than the untreated regular PMMA, indicating that ion

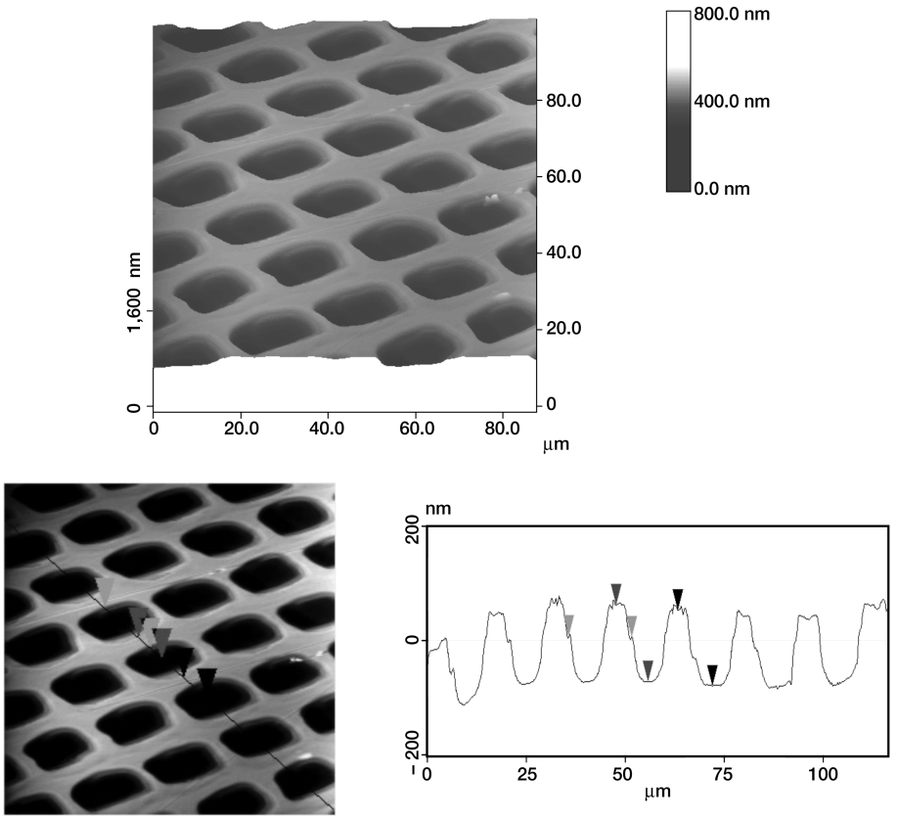

Fig. 3. *AFM images of the PMMA surfaces after exposure with 115 keV, 1×10^{15} ions/cm^2 Ar^+ ions, recorded in the tapping mode with typical surface features characterized by a cross section analysis.*

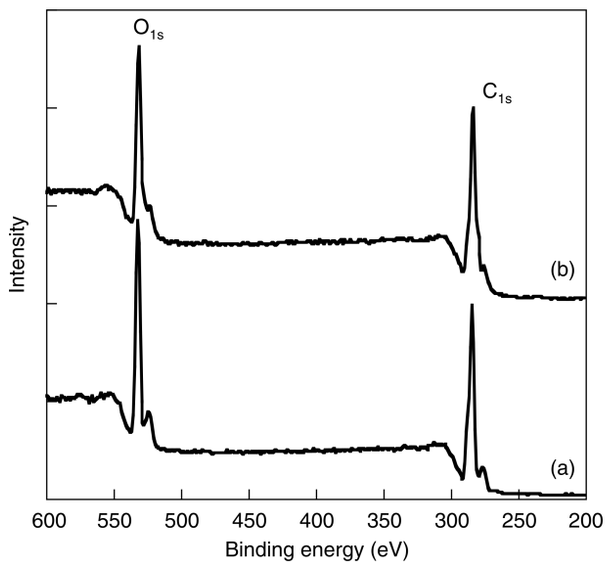

Fig. 4. *XPS survey spectra obtained from (a) pristine and (b) P^+ implanted sample with 1×10^{15}ions/cm^2.*

implantation does improve osteoblast adhesion on polymeric substrate, due to the increased surface roughness. This is consistent with what Webster and coworkers found in their studies, where strong correlations between increased surface roughness and enhanced osteoblast adhesion was demonstrated (Webster et al., 2001, and references therein). Although similar surface topography and surface roughness were observed for P^+ irradiated and Ar^+ irradiated PMMA films, the former has more cells attached than the latter, implying that surface morphology is not the only factor that promoted osteoblast adhesion, selection of ion species also is important for cell adhesion. Ar^+ ions are inert, but P^+ ions implanted to the polymeric substrate might have helped improve osteoblast adhesion. The distribution of P^+ ions on the PMMA film was determined by SIMS. Shown in Figure 6 is the dynamic SIMS depth profiling data for P in the treated PMMA film. The concentration of P ions vs. depth was displayed and the majority of P ions are distributed in the area that is about 100 nm from the surface. The maximum amount of P ions, 1.1×10^{20}/cm^3 was found at 121 nm.

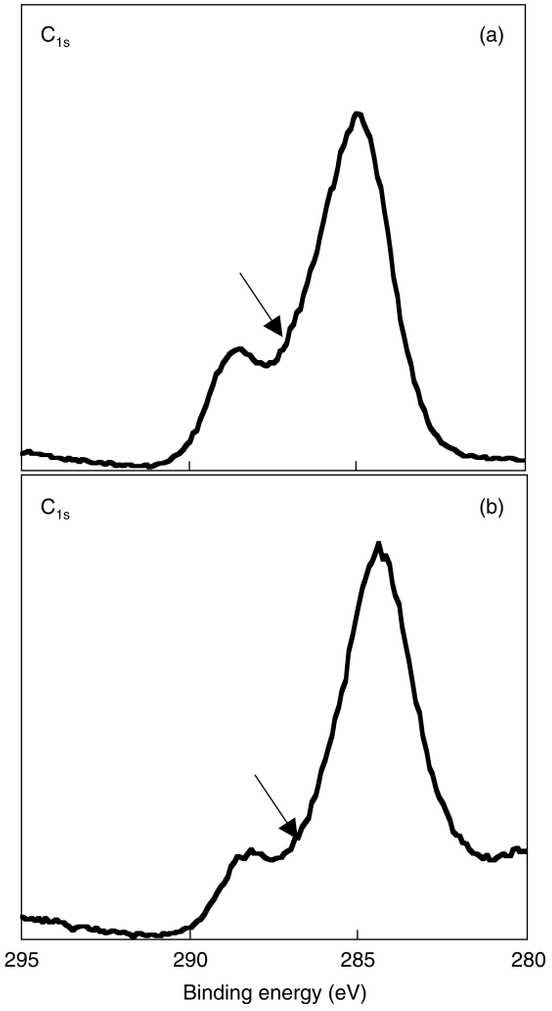

Fig. 5. *C_{ls} XPS survey spectra obtained from (a) pristine and (b) P^+ implanted sample with 1×10^{15} ions/cm^2.*

Table 1. *Surface roughness and the relative amount of osteoblast cells (R.O.) attached after 24 hours (refer to regular PMMA film, R.O. = 1)*

Ions	Energy (keV)	Dosage (ions/cm^2)	R_{rms} (nm)	R.O.
P	85	1×10^{15}	60.525	2.44
Ar	115	1×10^{15}	57.613	1.72

4. Conclusions

The results presented here demonstrate that masked ion beam lithography (MIBL) is a viable and novel technique for patterning and doping soft materials for potential biomedical applications. Compared with conventional patterning techniques, MIBL not only modifies surface topography of the material, but also changes the surface chemistry in the same process via incorporation of ions. This in turn affects the interactions between cells and the material. Therefore, the MIBL technique could offer a distinct advantage for bone tissue engineering scaffold fabrication. Recent studies have indicated that mesenchymal stem cell (MSC) differentiation along the osteoblast lineage is dependent upon calcium concentration in differentiation media. Therefore, bone tissue engineering using MSCs may be improved by controlling the local calcium ion concentration at the scaffold/cell interface through calcium ion implantation. 3-dimensional constructs of these micromachined polymers can be achieved by either lamination or rolling techniques.

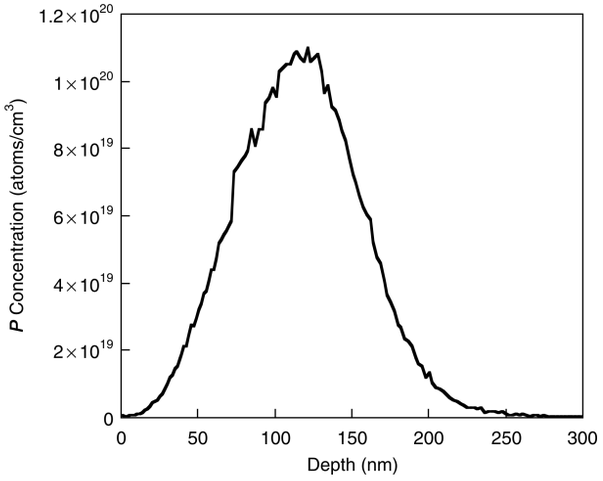

Fig. 6. *SIMS depth profile for P ions in PMMA after exposed to 85 keV, 1×10^{15} ions/cm^2 P^+ ion implantation.*

Acknowledgments

KEG acknowledges partial support from the North Carolina Biotechnology Center. NB was supported at UAM by a grant FIES-98-100-I (Instituto Mexicano del Petroleo, Mexico), and DP by the US Department of Energy under contract DE-AC05-00OR22725 with the Oak Ridge National Laboratory, managed by UT-Battelle, LLC.

References

C.M. Agrawal, JOM **50**(1), 31–35 (1998).
L. Bacakova, V. Svorcik, V. Rybka, I. Micek, V. Hnatowicz, V. Lisa, and F. Kocourek, Biomaterials **17**(11), 1121–1126 (1996).
V. Bianchi, R. Dal Toso, P. Debetto, and A.G. Levis, Toxicology **17**(2), 219–224 (1980).
M. Bosetti, A. Massè, E. Tobin, and M. Cannas, J. Mater. Sci.: Mater. Med. **12**(5), 431–435 (2001).
B.D. Boyan, T.W. Hummert, D.D. Dean, and Z. Schwartz, Biomaterials **17**, 137–146 (1996).

D. Buser, R.K. Schenk, S. Steinemann, J.P. Fiorellini, C.H. Fox, and H. Stich, J. Biomed. Mater. Res. **25**(7), 889–902 (1991).

B. Chehroudi, T.R. Gould, and D.M. Brunette, J. Biomed. Mater. Res. **23**(9), 1067–1085 (1989).

P.K. Chu, J.Y. Chen, L.P. Wang, and N. Huang, Mater. Sci. Eng. R **36**(5–6), 143–206 (2002).

B.A. Dalton, M. Dziegielewski, G. Johnson, P.A. Underwood, and J.G. Steele, BioTechniques **21**, 298–303 (1996).

D.A. Dwayne and M.L. McCain, J. Biomed. Mater. Res. **53**, 536–546 (2000).

C.H. Han, C.B. Johansson, A. Wennerberg, and T. Albrektsson, Clin. Oral Implants Res. **9**(1), 1–10 (1998).

T. Hanawa, Mater. Sci. Eng. A **267**, 260–266 (1999).

T. Hanawa, Y. Kamiura, S. Yamamoto, T. Kohgo, A. Amemiya, H. Ukai, K. Murakami, and K. Asaoka, J. Biomed. Mater. Res. **36**(1), 131–136 (1997).

T. Hanawa and M. Ota, Biomaterials **12**(8), 767–774 (1991).

T. Hanawa and M. Ota, Appl. Surf. Sci. **55**(4), 269–276 (1992).

T. Hanawa, H. Ukai, and K. Murakami, J. Electron Spectrosc. Relat. Phenom. **63**(4), 347–354 (1993).

W. He, D.B. Poker, K.E. Gonsalves, and N. Batina, Microelectronic Eng. (2002).

J.C. Heath and M. Webb, Br. J. Cancer **21**(4), 768–779 (1967).

D. Krupa, J. Baszkiewicz, J.A. Kozubowski, A. Barcz, J.W. Sobczak, A. Biliński, M. Lewandowska-Szumie, and B. Rajchel, Biomaterials **23**, 3329–3340 (2002).

M. Lampin, R. Warocquier-Clerout, C. Legris, M. Degrange, and M.F. Sigot-Luizard, J. Biomed. Mater. Res. **36**(1), 99–108 (1997).

C.T. Laurencin, A.M.A. Ambrosio, M.D. Borden, and J.A. Cooper, Jr. Annu. Rev. Biomed. Eng. **1**, 19–46 (1999).

T.Q. Lee, M.I. Danto, and W.C. Kim, Orthopedics **21**(8), 885–888 (1998).

J.E. Lemons, Surf. Coat. Technol. **103–104**, 135–137 (1998).

J.B. Lhoest, J.L. Dewez, and P. Bertrand, Nucl. Instr. Meth. B **105**, 322–327 (1995).

D.J. Li, F.Z. Cui, and H.Q. Gu, Nucl. Instr. Meth. B **152**, 80–88 (1999).

C. Maniatopoulos, R.M. Pilliar, and D.C. Smith, J. Biomed. Mater. Res. **20**(9), 1309–1333 (1986).

K. Murakami and K. Asaoka, J. Biomed. Mater. Res. **36**(1), 131–136 (1997).

Y. Nishi and R. Doering, *Handbook of Semiconductor Manufacturing Technology* (Marcel Dekker, New York, 2000).

B. Pignataro, E. Conte, A. Scandurra, and G. Marletta, Biomaterials **18**, 1461–1470 (1997).

W.K. Ramp, R.M. Dillaman, L.G. Lenz, D.M. Gay, R.D. Roer, and T.A. Ballard, Bone Miner. **15**, 1–17 (1991).

W.K. Ramp, L.G. Lenz, and K.K. Kaysinger, Bone Miner. **24**, 59–73 (1994).

A. Rich and A.K. Harris, J. Cell Sci. **50**, 1–7 (1981).

V.I. Sikavitsas, J.S. Temenoff, and A.G. Mikos, Biomaterials **22**, 2581–2593 (2001).

J.E. Sundgren, P. Bodö, B. Ivarssonand, and I. Lundström, J. Colloid Interface Sci. **113**(2), 530–543 (1986).

Y. Suzuki, M. Kusakabe, J.S. Lee, M. Kaibara, M. Iwaki, and H. Sasabe, Nucl. Instr. Meth. B **65**, 142–147 (1992).

V. Švorčík, K. Walachová, K. Prošková, B. Dvořánková, D. Vogtová, R. Öchsner, and H. Ryssel, J. Mater. Sci.: Mater. Med. **11**, 655–660 (2000).

K.A. Thomas and S.D. Cook, J. Biomed. Mater. Res. **19**(8), 875–901 (1985).

H.H. Trieu, J.R. Justis, T.D. Drewry, M.C. Sherman, B.J. Coates, and B.T. Estes, PCT Int. Appl. **2000**.

T.J. Webster, R.W. Siegel, and R. Bizios, Scripta Mater. **44**(8/9), 1639–1642 (2001).

A. Wennerberg, T. Albrektsson, and J. Lausmaa, J. Biomed. Mater. Res. **30**(2), 251–260 (1996).

J.F. Ziegler, J.P. Biersack, and U. Littmark, *The Stopping and Range of Ions in Solids* (Pergamon, New York, 1985).